University of Zurich[UZH]

Zurich Open Repository and Archive
University of Zurich
University Library
Strickhofstrasse 39
CH-8057 Zurich
www.zora.uzh.ch

Year: 2016

Change in streamflow response in unregulated catchments in Sweden over the last century

Åkesson, Anna ; Wörman, Anders ; Riml, Joakim ; Seibert, Jan

Abstract: A Fourier spectral analysis of daily discharge time series over the last century in 79 unregulated catchments in Sweden reveals a significant gradual steepening of the discharge power spectrum slope over time. Where historical meteorological observations are available (the 41 southernmost catchments), the results of our analyses indicate that local land use changes within the catchments have affected discharge power spectra to a greater extent than have changes in precipitation patterns. 1-D distributed routing analysis based on current and historical maps and scenario modeling in the Törnestorp Catchment suggests that changes in stream network properties have led to increases in the hydraulic Péclet number (math formula) and subsequent decreases in the discharge power spectrum over short periods. The analysis displays analytically how a change in stream network properties can result in changes in the power spectra, where the relative importance of the geomorphological and hydrodynamic dispersion effects determines the shape of the streamflow response. The lowering of the discharge power spectrum over short periods observed for many Swedish catchments is likely caused by increasing math formula (a decrease in dispersion) over time, resulting in higher peak values, especially for rapid streamflow responses (i.e., over short periods), demonstrated empirically for the Törnestorp case study. The finding that the discharge power spectrum can change significantly over time highlights the need for hydrological models to account for the effect of the nonstationarity of parameters that result from temporal change caused by land use change and/or climate change that is due to anthropogenic or natural causes.

DOI: https://doi.org/10.1002/2015WR018116

Posted at the Zurich Open Repository and Archive, University of Zurich
ZORA URL: https://doi.org/10.5167/uzh-132220
Journal Article
Published Version

Originally published at:
Åkesson, Anna; Wörman, Anders; Riml, Joakim; Seibert, Jan (2016). Change in streamflow response in unregulated catchments in Sweden over the last century. Water Resources Research, 52(8):5847-5867.
DOI: https://doi.org/10.1002/2015WR018116

AGU PUBLICATIONS

Water Resources Research

RESEARCH ARTICLE
10.1002/2015WR018116

Change in streamflow response in unregulated catchments in Sweden over the last century

Anna Åkesson[1], Anders Wörman[1], Joakim Riml[1], and Jan Seibert[2]

[1]Division of River Engineering, Royal Institute of Technology, Stockholm, Sweden, [2]Department of Geography, University of Zürich, Zürich, Switzerland

Key Points:
- Hydrograph variance has decreased significantly over the last century at short periods (days) in unregulated Swedish catchments
- Decreased hydrodynamic dispersion is a cause of the steepened discharge power spectra in Swedish catchments over the last century
- Analytical and numerical analyses show connection between power spectra and hydrodynamic as well as geomorphological dispersion effects

Supporting Information:
- Supporting Information S1
- Table S1
- Table S2

Correspondence to:
A. Åkesson,
anake@kth.se

Citation:
Åkesson, A., A. Wörman, J. Riml, and J. Seibert (2016), Change in streamflow response in unregulated catchments in Sweden over the last century, *Water Resour. Res.*, *52*, 5847–5867, doi:10.1002/2015WR018116.

Received 18 SEP 2015
Accepted 1 JUL 2016
Accepted article online 5 JUL 2016
Published online 5 AUG 2016

© 2016. American Geophysical Union. All Rights Reserved.

Abstract A Fourier spectral analysis of daily discharge time series over the last century in 79 unregulated catchments in Sweden reveals a significant gradual steepening of the discharge power spectrum slope over time. Where historical meteorological observations are available (the 41 southernmost catchments), the results of our analyses indicate that local land use changes within the catchments have affected discharge power spectra to a greater extent than have changes in precipitation patterns. 1-D distributed routing analysis based on current and historical maps and scenario modeling in the Törnestorp Catchment suggests that changes in stream network properties have led to increases in the hydraulic Péclet number (*Pe*) and subsequent decreases in the discharge power spectrum over short periods. The analysis displays analytically how a change in stream network properties can result in changes in the power spectra, where the relative importance of the geomorphological and hydrodynamic dispersion effects determines the shape of the streamflow response. The lowering of the discharge power spectrum over short periods observed for many Swedish catchments is likely caused by increasing *Pe* (a decrease in dispersion) over time, resulting in higher peak values, especially for rapid streamflow responses (i.e., over short periods), demonstrated empirically for the Törnestorp case study. The finding that the discharge power spectrum can change significantly over time highlights the need for hydrological models to account for the effect of the nonstationarity of parameters that result from temporal change caused by land use change and/or climate change that is due to anthropogenic or natural causes.

1. Introduction

The outflow hydrograph of a catchment is governed by climatic factors and hydrological processes that occur within the catchment. Hence, long-term and short-term changes in the dynamics of the outflow discharge of a catchment can result from changes in climatic and in catchment trends. Temporal changes in hydrologic mechanisms constitute a central issue pertaining to the pending hydrological decade (2013–2022) identified by the International Association of Hydrological Sciences (IAHS)—*Panta Rhei* [*Montanari et al.*, 2013].

Numerous studies have demonstrated that runoff patterns can vary considerably as a result of climate change [*Bergström et al.*, 2001; *Vörösmarty et al.*, 2000; *Xu*, 1999], land use change [*Mao and Cherkauer*, 2009; *Niehoff et al.*, 2002; *Zhang and Schilling*, 2006], or both [*Hirsch and Archfield*, 2015; *Jaramillo and Destouni*, 2014; *Wagener et al.*, 2010]. Whereas climate change has global impacts, land use change effects are generally local (catchment specific) [*Blöschl et al.*, 2015]. Despite vast efforts during the recent decades, hydrologic modeling including the effects of climate change [*Bergström et al.*, 2001; *Giorgi et al.*, 1994; *Montanari et al.*, 2013; *Teutschbein and Seibert*, 2013; *Xu*, 1999] as well as the effects of land use change [*Montanari et al.*, 2013] on river discharge patterns remain challenging issues. This study focuses solely on the latter topic.

Land use changes can occur in a multitude of manners and have been doing so in Sweden over the last century [*Cousins et al.*, 2015; *Ihse*, 1995; *Jepsen et al.*, 2015]. The present study focuses on the effects of changes in stream channel network properties over time and their effect on the streamflow response, i.e., how discharge hydrograph variations arise as consequences of the input precipitation time series. In agricultural land in Sweden, modifications of stream networks have generally involved installation of tile drainage on farmland and straightening and excavation of stream channels to increase the width of narrow cross sections and to eliminate thresholds that create backwater flow, i.e., to improve field drainage [*Salehin et al.*,

2003; *Wagener et al*., 2010]. Other land use changes outside the main scope of this study, which can significantly change the hydrograph variations, are issues related to thawing of permafrost [*Sjöberg et al*., 2012], forestry management [*Kløve and Bengtsson*, 1999], natural geomorphological processes (such as meandering of rivers and erosion), lowering of lake levels, the extension of urban areas with impervious surfaces and water-regulation issues such as construction of dams and/or water transfers between subcatchments.

In this study, Fourier spectral analysis is used to reveal the periodic nature of the discharge time series and to quantify spectral changes in hydrograph variations over the last century in unregulated catchments in Sweden. The spectral analysis is used to sort the fluctuations in the hydrograph over frequencies, which facilitates linkage of such sorted fluctuations to hydraulic-geomorphic processes acting on different time scales.

Travel time distributions of water or solutes are often used to describe the flow characteristics of a particular stream network (and/or catchment) [*Foster et al*., 2000; *McDonnell et al*., 2010; *Rinaldo et al*., 1991; *Saco and Kumar*, 2002; *Snell and Sivapalan*, 1994; *Viglione et al*., 2010]. Our understanding of the nonstationary mechanisms of hydrological systems remains very limited because of their complexity [*DeFries and Eshleman*, 2004; *Niehoff et al*., 2002; *Zhang and Schilling*, 2006]. Commonly one uses the instantaneous unit hydrograph (IUH) to represent the distribution of flow travel times in a catchment, which itself is constant over time but reflects a change of the temporal variance in the input of water mass to the effluence water mass discharge [*Dooge*, 1959; *Rodríguez-Iturbe and Valdés*, 1979; *Snell and Sivapalan*, 1994; *Troutman and Karlinger*, 1984]. Since the power spectrum, resulting from the Fourier spectral analysis, represents the distribution of variance in discharge on frequency, changes in the power spectrum of discharge over long times may reflect changes in the IUH. In this paper, we establish the relationship between the IUH and the power spectrum of the discharge time series at the effluence of a catchment. By investigating the gradual change in the power spectrum in historical discharge monitoring time series over long times, it should be possible to link those changes to changes in the IUH and the stream channel network properties. In the case that the power spectrum of discharge exhibit monotonical, systematic variation over frequency, for instance a fractal distribution, it would be possible to quantify the change in the spectrum by using its slope. Furthermore, such changes in the power spectrum slope can be coupled to specific features in discharge time series like peak flows which will be described in this paper.

By use of a distributed 1-D hydraulic routing model, the impacts of different stream network properties on stream travel times and resulting hydrographs are analyzed. The goal is to quantify how potential changes within the stream network may be related to temporal changes in discharge statistics. Although anthropogenic effects of land use change can occur in any part of a catchment, this study exclusively considers potential changes in stream network properties. Focus is put on the shorter time scales of the hydrograph variations to ultimately develop a stronger understanding of the in-stream hydraulic mechanisms.

2. Methodology

The study and the analyses of temporal changes in hydrograph variations due to land use changes are structured as follows. First, the outcomes of the analyses of temporal changes in the power spectra of the discharge series in 79 unregulated (or moderately regulated) Swedish catchments are described. The temporal changes in precipitation are eliminated from the power spectra to determine whether the temporal changes in the power spectra of the catchment flow response differ from the temporal changes in the discharge power spectra. This latter analysis is performed for 41 catchments in southern Sweden for which adequate precipitation records were available. Thereafter, a theoretical framework is presented and developed to clarify how stream network properties and processes may influence the discharge power spectra. Finally, a routing analysis is performed for the case study catchment, Törnestorp, to quantitatively investigate how anthropogenic modifications to stream networks in agricultural landscapes may have influenced the in-stream travel time.

2.1. Spectral Analyses of the Streamflow Response

Discharge time series that are publicly available from the Swedish Meteorological Institute (SMHI) were collected for all catchments that are considered to be unregulated or moderately regulated according to the SMHI's classification. Observational records that are equal to or longer than 55 years were included. This

arbitrarily chosen threshold was designed to include discharge measurement stations from the 1950s, when the national observational network was expanded. Using these criteria, we generated a list of 79 catchments covering an area of approximately 131,000 km^2, corresponding to approximately 29% of Sweden's land area (although a few catchments partially extend into Norway and/or Finland).

The average and median length of the daily discharge time series were both 83 years. Twenty-three of the 79 discharge time series extend back more than 100 years, and the longest discharge series covers a 110 year period. The catchment areas range from 1.6 to 33,930 km^2, the average catchment area is 2463 km^2, and the median area is 687 km^2. All rivers meet the criteria of being regulated only to a small degree and some small catchments used in the analysis sometimes overlap with larger catchments, as shown in the map representations in Figure 4.

By comparing the spectral power of time series (for example, with regard to discharge, precipitation and solutes) at different periods, patterns of attenuation over time for respective time scales can be revealed [*Basu et al*., 2011; *Kirchner*, 2009; *Riml and Wörman*, 2015; *Wörman et al*., 2010]. Through Fourier spectral analyses, the hydrograph can be separated into frequency-specific (constant) amplitudes over the selected time series [*Dolgonosov et al*., 2008; *Kirchner et al*., 2000; *Riml and Wörman*, 2015; *Wang et al*., 2008; *Wörman et al*., 2010].

Because various hydraulic and geomorphologic processes act on different time scales, one can expect to find a variable impact and importance of these processes over a range of periods (defined as the inverse of the frequency). The power spectrum analysis can be interpreted in the context of relative importance of variance at different periods, and thus give an indication of the degree of randomness in the time series. The time series were detrended, filtered by Hamming windowing and power spectra were calculated according to Welch's method (using the Matlab® software). Hamming windowing was applied to minimize the effects of discontinuities at the limits of the time series.

2.1.1. Catchment Flow Response Power Spectrum

2.1.1.1. Evaluation of Spectral Trends From Historical Data

The discharge time series (of daily measurements) is continuous for every half-year, and the length of the records is appropriate for the purposes of the study, which is to test the hypothesis that (anthropogenic) land use changes have had substantial effects on the hydrograph variations. To reduce (and for southern Sweden, to eliminate) the effects of accumulation of snow, a nonlinear process that can have a substantial influence on the hydrograph variations, only the May-to-October period was analyzed for each year. To examine the implications of nonstationary (transient) time series and transient power spectrum, other options are viable [*Benettin et al*., 2015; *Harman*, 2015; *Kirchner*, 2009; *Palanisamy and Workman*, 2014; *Steinschneider and Brown*, 2013; *Torrence and Compo*, 1998].

All years that included gaps in the discharge series were eliminated. The Fourier discharge power spectrum $S_{Q,j}$ (m^6) for every year j (according to the Julian calendar) in the available time series was fitted to a power law distribution with the following form:

$$S_{Q,j}(T) = a_{Q,j} T^{b_{Q,j}} \tag{1}$$

The evaluated coefficients $a_{Q,j}$ and $b_{Q,j}$ describe the yearly spectral level and slope of the spectrum, respectively, and T denotes the period (days). The regression was based on equation (1):

$$\ln\left(S_{Q,j}(T)\right) = \ln\left(a_{Q,j}\right) + b_{Q,j}\ln\left(T\right) \tag{2}$$

To evaluate potential changes in the power spectral level and slope over time, the calculated coefficients for yearly spectrum levels ($a_{Q,j}$) and spectral slopes ($b_{Q,j}$) were fitted using linear regression:

$$a_{Q,j} = k_{a,Q} \cdot j + m_{a,Q} \tag{3}$$

and

$$b_{Q,j} = k_{b,Q} \cdot j + m_{b,Q} \tag{4}$$

giving rise to the coefficients $k_{a,Q}$, $m_{a,Q}$, $k_{b,Q}$, and $m_{b,Q}$ for each of the 79 catchments.

Additional analyses were conducted to eliminate effects of temporal changes in the precipitation power spectrum of a nearby meteorological station from the discharge power spectrum. Outflow from the

catchment, Q (m^3/s), can, according to the IUH theory [*Dooge*, 1959; *Rodríguez-Iturbe and Valdés*, 1979; *Snell and Sivapalan*, 1994; *Troutman and Karlinger*, 1984], be obtained by convolving a precipitation time series with the catchment flow response based on

$$Q(t)=\int_0^\infty \Big(P(\tau)-ET(\tau)\Big) f_C(t-\tau)d\tau \tag{5}$$

where P is the precipitation load to the catchment (m^3/s), ET is the evapotranspiration (m^3/s), and f_C is the catchment flow response function. f_C thus includes all the mechanisms that transforms the input signal (rainfall minus evapotranspiration) to catchment outlet discharge: hillslope runoff, groundwater flow as well as stream channel flow, i.e., the IUH (s^{-1}).

The function f_C describes the unit response of a linear system based on an assumption of stationary parameters. Equation (5) and the following argumentation are based on the linear assumption—i.e., that nonlinear processes are subordinate to the linear processes in shaping the daily hydrographs for the summer half-year.

Equation (5) allows for a transformation that utilizes convolution in the time domain, which corresponds to multiplication in the Fourier domain. This implies that the power spectrum of the catchment flow response can be separated from the boundary conditions consisting of the precipitation and evapotranspiration in the form of

$$S_{Q,j}(T)=\Big(S_{P,j}(T)+S_{ET,j}(T)-2C_{P,j:ET,j}\Big)\ S_{f,C,j}(T) \tag{6}$$

where S denotes the Fourier power spectrum of a given parameter, and C denotes the coherence spectrum. Generally, the variance in evapotranspiration is much smaller than the variance in precipitation, which implies that $S_{P,j}(T) \gg |S_{ET,j}(T)-2C_{P,j:ET,j}|$. Hence, the power spectrum of the catchment flow response, the so-called spectral scaling function [*Riml and Wörman*, 2015], $S_{f,C,j}(T)$, that reflects the properties of the catchment can be evaluated numerically as

$$S_{f,C,j}(T)=S_{Q,j}(T)S_{P,j}(T)^{-1} \tag{7}$$

where $S_{f,C,j}$ is a scaling function that consists of the properties of the catchment.

For those years when daily observations of both precipitation and discharge time series were available, the spectral scaling function was fitted to a line of the following form:

$$S_{f,C,j}(T)=a_{C,j}\cdot T^{b_{C,j}} \tag{8}$$

where the regression was based on

$$\ln\left(S_{f,C,j}(T)\right)=\ln\left(a_{C,j}\right)+b_{C,j}\ln\left(T\right) \tag{9}$$

The calculated spectral levels and spectral slopes were plotted for each year, and a linear fit was generated such that

$$a_{C,j}=k_{a,C}\cdot j+m_{a,C} \tag{10}$$

and

$$b_{C,j}=k_{b,C}\cdot j+m_{b,C} \tag{11}$$

yielding the coefficients $k_{a,C}$, $m_{a,C}$, $k_{b,C}$, and $m_{b,C}$ for the 41 catchments for which both historical discharge and precipitation series were available. For the precipitation power spectrum, the analogous indices are labeled as P; thus, the coefficients of the fit of the precipitation spectral level and slope are denoted as $k_{a,P}$, $m_{a,P}$, $k_{b,P}$, $m_{b,P}$, $a_{P,j}$, and $b_{P,j}$, respectively.

2.1.1.2. Statistical Analyses of Spectral Trends

For every catchment, the slopes b_Q and b_C were determined from the discharge power spectra of the May-to-October period of each year using the least square method. Further, the trends in b_Q and b_C and their

confidence bounds were evaluated over the years, using *t*-statistics as defined by the slopes $k_{b,Q}$ in equation (4) and $k_{b,C}$ in equation (11). If both bounds of $k_{b,Q}$ (or $k_{b,C}$) are positive on a 95% confidence level it means that there is a statistically significant positive trend in the slope b_Q (or b_C).

2.1.2. Stream Network Flow Response Power Spectrum

2.1.2.1. Evaluation of a Numerical Hydrological Model

Using a hydrological model (here the HBV model, see section 2.3), the stream network response function f_N can (in analogy with equation (5)) be determined as

$$Q_{out}(t) = \int_0^\infty (Q_{in}(\tau)) f_N(t-\tau) d\tau \tag{12}$$

where Q_{in} is the (modeled) inflow to the stream network and Q_{out} is the (modeled) outflow from the stream network. Hence, f_N gives a possibility to evaluate the processes in the stream network that reshapes the hydrograph during its passage through the stream network.

The stream network scaling function, $S_{f,N}(T)$, can be evaluated numerically, as a function of the power spectrum of the modeled outflow (Q_{out}) from the stream network $S_{Q,out}$ and the power spectrum of the modeled inflow (Q_{in}) into the stream network $S_{Q,in}$:

$$S_{f,N}(T) = S_{Q,out}(T) S_{Q,in}(T)^{-1} \tag{13}$$

By determining the scaling factor for different stream network property conditions (scenarios), the change in stream network's effect on the hydrographs can be quantitatively evaluated. Note that for this purpose (in contrast with our catchment flow response analyses) daily discharge values over a time frame of many years, was used.

2.1.2.2. Analytical Solution to the Spectral Scaling Function

The stream network flow response function can be represented by the kinematic-diffusive wave model in a network of 1-D surficial flow paths, i.e., a linear form of the wave equation [*Rinaldo et al.*, 1991; *Wörman et al.*, 2010]. By assuming a gamma distributed network of flow paths, the scaling function can thus be formulated as follow (after the methodology of *Riml and Wörman* [2015]):

$$S_{f,N}(T) = \left[1 + \left(\frac{u}{2D_L\beta_\gamma}\right)^2 \left(-1 + \sqrt{1 + 16\frac{D_L^2}{u^4T^2}}\right)\right]^{-\alpha_\gamma} \tag{14}$$

where u is the flow velocity (m/s), D_L is the longitudinal hydrodynamical dispersion (m^2/s), and T is the period (s). α_γ and β_γ (m^{-1}) are the shape and scale parameters of the gamma distribution that defines the distribution of transport distances, i.e., the topology of the network.

According to equation (14), the scaling function will be defined by several factors associated with the geomorphologic and hydrodynamic properties of the stream network, of which only some are dependent on period. Similarly, the stream network flow response based on the same model representation can be solved analytically by transforming the solution to the Laplace domain. Thus, the stream network flow response becomes

$$\bar{f}_N(s) = \left[1 + \frac{u}{2D_L\beta_\gamma}\left(-1 + \sqrt{1 + \frac{4sD_L}{u^2}}\right)\right]^{-\alpha_\gamma} \tag{15}$$

where $\bar{f}$ is the Laplace transformed instantaneous unit hydrograph and s is the Laplace operator.

While equations (14) and (15) offer exact solutions to the stream network flow response, which can be generalized to flow paths over the entire catchment, equation (8) is used herein to simplify the investigation of the change in the two parameters a_c and b_c over time. In the discussion section however, equations (14) and (15) are utilized to provide a physical explanation of the temporal change in catchment scaling function in terms of stream network properties.

2.2. Distributed Hydraulic Routing in One Case Study Catchment

2.2.1. Distributed Routing Model

A 1-D distributed routing model applied in previous studies [*Åkesson et al.*, 2015; *Åkesson and Wörman*, 2012] and based on the steady state form of the 1-D longitudinal Saint-Venant equations for shallow water

flow was set up for different sets of stream network properties in an agricultural catchment in southern Sweden. The various sets of properties are denoted *scenarios* and were designed to represent potential anthropogenic modifications of stream network properties.

The model accounts for nonuniform flows associated with backwater effects, which can substantially affect streamflow responses [*Chow et al*., 1988; *Liu et al*., 2003]. For each stream reach and flow, the flow state (supercritical or subcritical) was determined. For supercritical conditions, normal depths were assumed to prevail along the entire reach with constant channel properties. For subcritical conditions, nonuniform velocities (and, consequently, water levels) along the reach were determined using an iterative central finite difference method to calculate the slope of the energy line. The calculation was performed stepwise in the upstream direction from the stream network outlet toward its sources. Friction head loss in the reaches was calculated using the Manning equation and combined with the steady state form of the 1-D momentum equation via the so-called step method. When a reach was deemed subcritical for the given conditions and the associated downstream reach was supercritical, the critical depth downstream was used as the lower boundary condition for the calculation. In other cases, when the downstream reach was also subcritical, the actual depth at the upstream end of the downstream reach was used as the boundary condition.

The model can account for backwater effects, because a numerical discretization shorter than the reach lengths Δx is used throughout the calculations. Hence, the slope of the energy line does not need to be constant within a stream reach; for example, even if the downstream end of a reach is subcritical, a hydraulic jump can occur within the reach such that the upstream end of the reach is supercritical. Apart from identifying a spatial calculation increment that is sufficiently small to ensure a stable (converging) solution, the model is not explicitly calibrated. Given the limited availability of data regarding stream network properties, generic parameters were used to examine properties such as stream channel geometries.

For all of the modeling scenarios, Manning's friction coefficient (n) was assumed to be 0.05 s/m$^{1/3}$ [*Arcement and Schneider*, 1989; *Chow et al*., 1988; *French*, 2007; *Schulze et al*., 2005] as an intermediate value of common friction coefficients in natural catchments. Hydraulic models are generally highly sensitive to river roughness values; however, models that include backwater flows (such as the model used here) are less sensitive to the friction coefficient because geomorphological properties that generate damming sections have substantial effects on the travel times [*Åkesson et al*., 2015; *Åkesson and Wörman*, 2012; *Liu et al*., 2003; *Schulze et al*., 2005]. The downstream energy levels at the catchment outlet were set to be constant at 5 m above the threshold at the stream network outlet to ensure an unambiguous relationship between the average travel time and discharge.

By determining the streamflow velocity of each stream reach at various discharges and knowing the stream reach length, the total travel time within the stream network can be determined. The influence of different stream network properties (simulated here through the use of several different scenarios) on the distribution of the ensemble of travel times is later used to assess the influence of different stream network properties on the discharge hydrograph.

To obtain an unambiguous relationship between the travel time and discharge, the distributed stream network routing model is designed for discrete values of network discharge (assuming quasi-stationary conditions), thus generating average advective travel times through a stream network that vary with discharge (stage). In reality, an unambiguous relationship between the travel times and catchment outlet discharge does not exist because of the presence of nonstationary conditions in the stream network. The quasi-stationary approach serves as a means of understanding variations in streamflow responses with varying discharge and stream network properties and is commonly used in runoff modeling [*McDonnell et al*., 2010].

2.2.2. The Törnestorp Catchment

The Törnestorp Catchment, which is located in southern Sweden in the Västergötland region and represents one of the most agriculturally intensive areas in Sweden, was selected for a more in-depth analysis of changes in streamflow response. The selection criteria were several, e.g., adequate sizing: small enough to reasonably enable distributed stream network modeling but large enough to allow stream network mechanisms to substantially impact the streamflow responses. Additionally, we sought a catchment with a low lake area percentage, a high ratio of agricultural land at present, available maps (present day as well as historical) and long-term series of discharge, precipitation and temperature observations. The catchment covers an area of 167 km^2 and contains only 0.7% lake or wetland areas and 52% agricultural areas; thus, this

catchment includes the highest percentage of agricultural land among all of the 79 catchments used in the spectral analyses. The stream network is classified as unregulated according to SMHI. The nearby Skara meteorological station, for which meteorological records are available from 1 January 1879, provided the input data for the HBV model. The meteorological station is located approximately 30 km from both the discharge station in Törnestorp and the center of the catchment.

2.2.3. Scenario Modeling

The various modeling scenarios consisted of all combinations of the following factors, resulting in 36 different modeling scenarios of the physical properties in the Törnestorp stream network.

1. Stream network coordinates:
   a. Historical map (the 1880s).
   b. Overview map (circa 2014).
   c. Terrain map (circa 2014).
2. Floodplain angle toward horizontal plane:
   a. 5° (floodplain case).
   b. 90° (bounded case, i.e., no flooding).
3. Channel width:
   a. uniformly increasing, i.e., scaled with discharge and increasing toward the outlet and
   b. randomly varying.
4. Stream reach discretization:
   a. ∼10 m.
   b. ∼50 m.
   c. ∼100 m.

2.2.3.1. Stream Network Coordinates

Geographical data, including the stream network coordinates and catchment delineation, were obtained from the Swedish water archive at the SMHI from 2012 [*Lindström et al*., 2010] based on the 1:250,000 scale overview map. For higher resolution stream network coordinates, data from the Terrain map (*Terrängkartan*), which also represent the present-day conditions at a scale of 1:50,000, were also used. For our historical maps, the District Economic map series (*Häradsekonomiska kartan*) of the Geographical Survey Office archive (Rikets allmänna kartverks arkiv) available from the Swedish mapping, cadastral and land registration authority (*Lantmäteriet*) was used. The historical map for the Törnestorp Catchment was constructed during the 1877–1882 period. Stream networks from the terrain and historical maps were digitized manually using ArcMap 10.2® because the stream network coordinates were not available as vector data. It was assumed that the catchment delineation has not changed over time. An excerpt from the three different maps is presented in Figure 1 alongside a map illustrating the location of the Törnestorp Catchment in Sweden (in red).

2.2.3.2. Floodplain Angle Toward the Horizontal Plane

The channel cross-sectional geometries were estimated in a generic manner and scaled based on the average discharge for every reach. The stream cross-sectional geometries were approximated based on rectangular main channels using the channel bottom width w (m) and channel depth r (m). At the main channel depth r, the main channels are surrounded by sloping floodplains at an angle of $\beta = 5^\circ$ (denoted as *the floodplain case*) slanted toward the horizontal plane or surrounded by vertical walls (levees), i.e., $\beta = 90^\circ$ (denoted as *the bounded case*), thus implying that the stream overflows its banks if the water levels exceed the main channel depth r in the floodplain case. The actual geometry is generally expected to fall between the floodplain and bounded generic cross-sectional shapes, which represent two fundamentally different extremes.

The generic dimensioning of the cross-sectional geometries was based on a field campaign conducted in the Heåkra Catchment of the Scania region in 2009 [*Åkesson and Wörman*, 2012]. Because the two catchments (Heåkra and Törnestorp) appear to be similar in terms of average discharge, size, average slopes, agricultural and lake percentages, among other characteristics, we made the assumption that the cross sections in Törnestorp could generically be approximated by the geometric relationships derived from the 170 measured cross sections in Heåkra. The cross-sectional geometries of the reaches in Törnestorp Catchment were designed to be uniformly scaled with the average discharge in respective reach to make the cross sections wider and deeper with increasing average discharge (i.e., toward the outlet). The channel dimensions of the reaches were determined as $r = C_r \cdot Q_{average}$ for the channel depth and $w = C_w \cdot r$ for the channel width, with

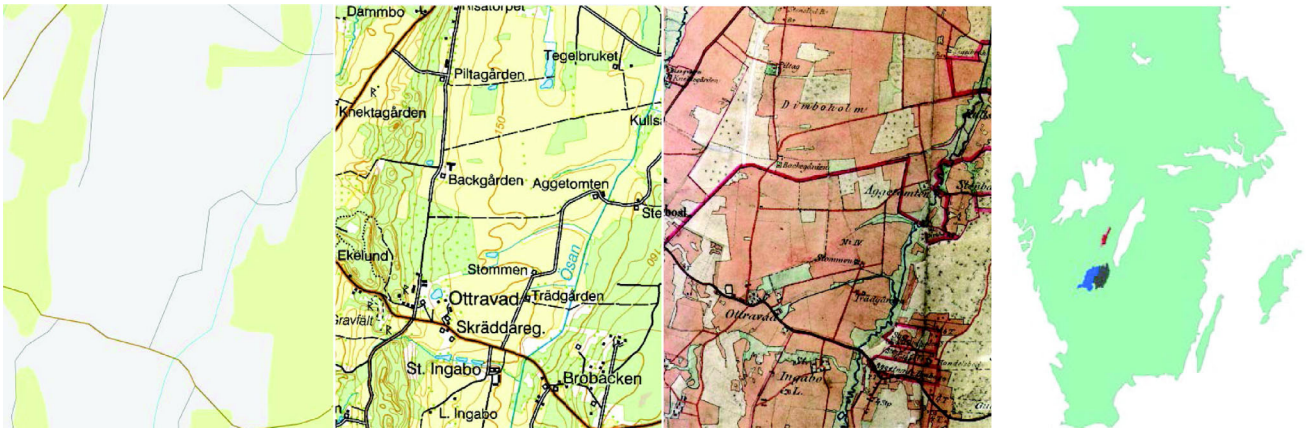

Figure 1. Parts of the Törnestorp Catchment according to the three different map representations, from left: the overview map (the 2010s), the terrain map (the 2010s), and the historical map (Häradsekonomiska kartan, the 1880s). The subplot on the right shows the locations of the Törnestorp (red) and Assmebro and Nissafors Catchments (blue and grey, respectively).

the coefficients C_r and C_w being numerically determined from the measured cross sections in Heåkra Catchment.

The validity of the coefficients C_r and C_w was tested in Heåkra, indicating that most of the 170 measured cross sections in the Heåkra Catchment could be considered as intermediates of the generic cross sections (floodplain and bounded) with respect to how the cross-sectional area, hydraulic radius, and wetted perimeter varied by stage [see *Åkesson and Wörman*, 2012, Figure 8].

2.2.3.3. Channel Width

To determine the potential effects of anthropogenic stream widening, an additional scenario in which the stream widths were also dimensioned in a more randomized manner (i.e., not automatically widening toward the catchment outlet) was considered. Although the same values as those presented above were used for the channel depth, the stream width was randomly determined using the following relationship: $w_{rand} = w \cdot (1 + rand)$, where the random variable *rand* was generated in MATLAB® such that $-0.75 \leq rand \leq 0.75$. The outcomes of this randomized approach for assigning channel properties are visualized in the right subplot of Figure 2.

2.2.3.4. Stream Reach Discretization

Within each stream reach, properties such as the cross-sectional channel geometries and bottom slopes remain constant. The topographical data used were rasterized DEM data with a resolution of 50 × 50 m, and the elevation at the start point of each reach in the stream network was determined through interpolation. The three different stream network representations were discretized into stream reaches that

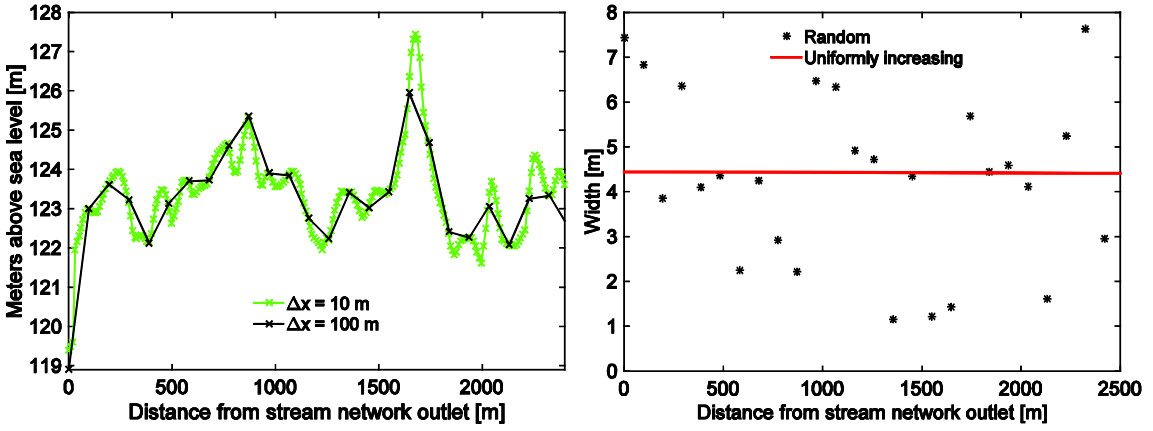

Figure 2. The plot on the left shows variations in streambed elevation due to stream reach discretization for the terrain map. In the plot on the right, different assumptions regarding channel width are demonstrated, with the red line indicating a uniform width scaled with discharge (increasing slightly toward the outlet) and the black line more randomized assignment of channel properties.

represent three different resolutions; the stream network was divided into reaches with approximate resolutions of $\Delta x = 10$ m, $\Delta x = 50$ m, and $\Delta x = 100$ m. The total network length X (m) was divided into N reaches, where N is the integer value that provides an actual reach length that is as close as possible to Δx.

The subplot on the left side of Figure 2 demonstrates that whereas the topographic gradient over the entire catchment is the same for all of the studied alternatives, the stream reach discretization substantially affects the local bottom slopes, where a lower spatial resolution (e.g., $\Delta x = 100$ m) generates smoother stream topography (black).

2.3. Hydrologic Modeling

To model the transformation of precipitation to water entering the stream network a bucket-type, lumped model was used. The widely used HBV model [*Bergström*, 1973; *Lindström et al*., 1997] was used here in the software implementation HBV light [*Seibert and Vis*, 2012]. The HBV model consists of different routines that represent processes related to snow, soil water, groundwater, and streamflow routing. Typically, 10–15 free parameters are used within these different routines. The HBV model was calibrated based on a 30 year period spanning from 1 October 1984 to 30 September 2014, which was preceded by a 2 year warming-up period. A generic algorithm [*Seibert*, 2000] was used for automatic optimization purposes, and the optimized parameter sets were used to simulate the entire period for which meteorological records exist.

The streamflow response, i.e., the routing mechanisms within the stream network that transform the inflow hydrograph to the outflow hydrograph, was simulated in two different ways: (i) using the built-in routing function of the HBV model and (ii) using a physically based stream network flow response function based on hydromechanical modeling of the stream networks. The inflow to the streamflow compartment, modeled by the HBV model is denoted as Q_{in} (m^3/s), and the modeled catchment outflow hydrograph using the built-in routing function is denoted as Q_{HBV} (m^3/s) whereas the outflow hydrograph based on hydromechanical modeling was denoted $Q_{physical}$ (m^3/s). The different inflow and outflow hydrographs are needed to be able to compare the power spectra of the inflow and outflow series (where the difference between these two signals is caused by the in-stream processes). Another point was to be able to compare the effect of different stream network flow responses; i.e., HBV vs physically based, as well as a comparison between the different scenarios of the stream network routing, in terms of their power spectra.

The performance of each implemented flow response function was evaluated in terms of its Nash-Sutcliffe Efficiency (R_{eff}) to compare the performance of each model [*Nash and Sutcliffe*, 1970].

2.3.1. HBV Model Application

The streamflow routing mechanism of the HBV model is a transformation function that is governed by the empirically determined MAXBAS parameter, which can be interpreted to define the travel time distribution of a floodwave through a stream network [*Lindström et al*., 1997]. The MAXBAS parameter is a triangular weighting function that distributes generated runoff over time [*Seibert*, 1997] . The MAXBAS (days) parameter was calibrated to approximately 3 days in the Törnestorp Catchment for the case study, and the HBV modeling was performed for the same years as for which discharge measurements were available for the Törnestorp case study catchment (1956–2014).

2.3.2. Physically Based Stream Network Flow Response Functions

For the distributed routing, the discharge in every stream reach was needed. The inflow to the stream network was distributed uniformly across an orthogonal grid (the grid size used has a resolution of 25 m) over the catchment area. From the point of distribution (i.e., the impact point of precipitation), every unit source term enters the stream network into the closest (by Euclidian distance) reach [*Åkesson and Wörman*, 2012]. Because the discharge in every reach is proportional to the sources that drain into the reach (lateral inflow) and that are added to the inflow from upstream reach(es), it increases toward the catchment outlet.

The physically based streamflow routing routine [*Åkesson et al*., 2015; *Åkesson and Wörman*, 2012] uses the concept of a linear reservoir, i.e., a first-order transfer relationship between the outflow discharge $Q_{physical,i}$ (m^3/s) and water volume V (m^3) within the stream network.

$$Q_{physical,i} = \frac{1}{|\tau_i(Q_{in,i})|} \cdot V_i = \alpha_i(Q_{in,i}) \cdot V_i \quad (16)$$

where $\langle \ldots \rangle$ denotes the arithmetical average and τ denotes the travel time (s) of the water. Consequently, the stage-dependent rate coefficient α_i (s^{-1}) can be defined as the inverse of the average travel time at the inflow discharge at time step i. As the travel time τ varied between the 36 different scenarios (see section 2.2.3), each scenario generated an individual outflow hydrograph, which were compared in terms of their power spectra.

3. Results

3.1. Spectral Analyses

The discharge power spectrum was determined for the May-to-October period for all of the 79 catchments and for each year that discharge records were available. For different catchments, the slopes of the discharge power spectra were found to vary over time in different ways, as exemplified in Figure 3, which presents the averaged discharge power spectrum for two neighboring catchments. The two catchments, Nissafors and Assmebro, are located in southwestern Sweden, as shown by the grey and blue areas, respectively, in the right of Figure 1.

To facilitate data analysis for most of the available time period, the decadal averages of the discharge power spectrum were determined for the period 1933–2013, over which consecutive observations were available for both catchments. The last time span ("decade") consisted of 11 years to utilize all of the available data. For the Assmebro Catchment, the discharge spectrum does not change gradually over the entire time period for which data are available. However, for the nearby Nissafors Catchment, the discharge power spectrum is noticeably flatter during the first part of the time period (the first four decades) than during the latter time period.

The changes in the slope of the discharge power spectrum over time, i.e., $k_{b,Q}$, for the 79 investigated catchments are displayed in Figure 4. Tables of the coefficients $k_{b,Q}$, $m_{b,Q}$, $k_{b,C}$, and $m_{b,C}$; as well as the analyzed time periods, and whether or not the change is significant for all catchments can be found in the supporting information. The analysis reveals a statistically significant change (at the 95% confidence level) in the discharge power spectral slope for 63 of the 79 studied catchments, of which 58 exhibit a positive change (increasing $k_{b,Q}$). At the extent of the entire country and all 79 catchments, the average coefficient for the temporal change in power spectral slope (i.e., "the slope of the slope") is $k_{b,Q}=0.00556$, a change that is statistically significant (the confidence level is 0.0043–0.0068) at the 95% confidence level, based on t test statistics. These results confirm the hypothesis that overall, a temporal change in streamflow response has

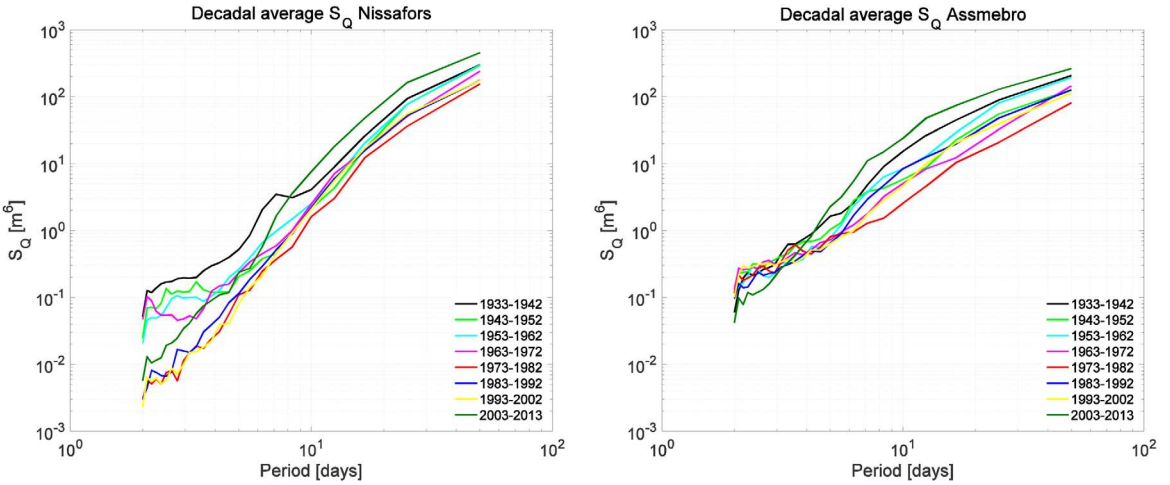

Figure 3. Averaging over decades reveals a steepening in the slope of the discharge power spectrum of (left) the Nissafors Catchment, whereas (right) the Assmebro Catchment displays similar slopes and levels for all decades.

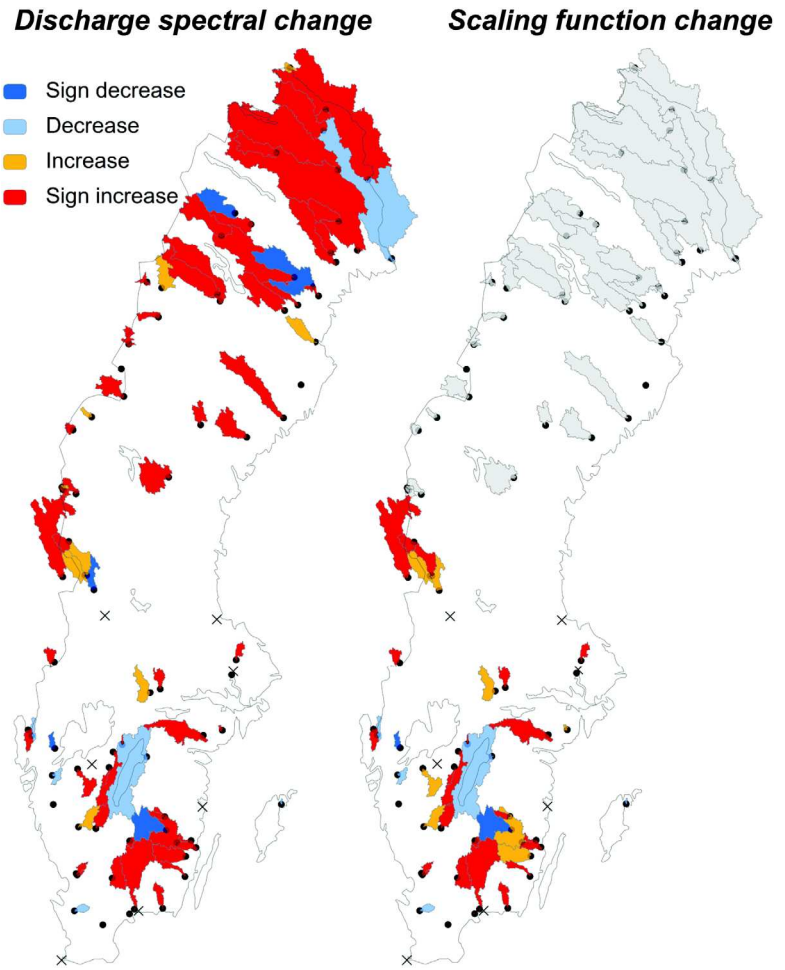

Figure 4. (left) Temporal change in the discharge spectral slope ($k_{b,Q}$) for 79 unregulated catchments in Sweden (right) in addition to the change in scaling function slope ($k_{b,C}$) for the 41 catchments for which historical meteorological records were available within a 150 km radius. Sign increase/decrease denotes the changes that are significant at the 95% confidence level. The dots mark the locations of the discharge measurement stations, and grey areas denotes catchments in which slopes were not calculated. In the case of overlapping (nested) catchments, the smaller subcatchments are plotted on top of the main catchments such that all catchments are visible.

occurred over the last century, as revealed here by a gradual steepening of the discharge power spectrum, in agreement with previous studies [*Wörman et al*., 2010].

The temporal changes in the discharge power spectrum and the catchment scaling function for the two neighboring catchments Nissafors and Assmebro (previously discussed in Figure 3) in Southern Sweden were compared (Figure 5). The linear trends (equations (2), (3), (10), and (11)) of the power law relationship were used to approximate the power spectrum of discharge, although many other possibilities exist. Their close spatial proximity and topographic similarities support the assumption that these catchments have experienced and continue to experience fairly similar climatic conditions.

Figure 5 shows that the spectral slope of the catchment scaling function of the Nissafors Catchment increases over time with, $k_{b,C} \approx 0.018$, whereas the neighboring catchment exhibits a relatively constant value (i.e., $k_{b,C} \approx 0.0005$). The change in the precipitation power spectrum over the same time period is minor and nonsignificant, and the slope of the catchment scaling function has increased similarly to the slope of the discharge power spectrum. Thus, it does not appear that nearby catchments, even ones of similar sizes and experiencing similar climatic conditions, such as Nissafors and Assmebro, always seem to have undergone similar temporal changes in terms of streamflow response.

The temporal changes in the slope of the catchment scaling function, i.e., $k_{b,C}$, for the 41 catchments in southern Sweden presented in Figure 4 (right) were however shown to be similar to the temporal changes

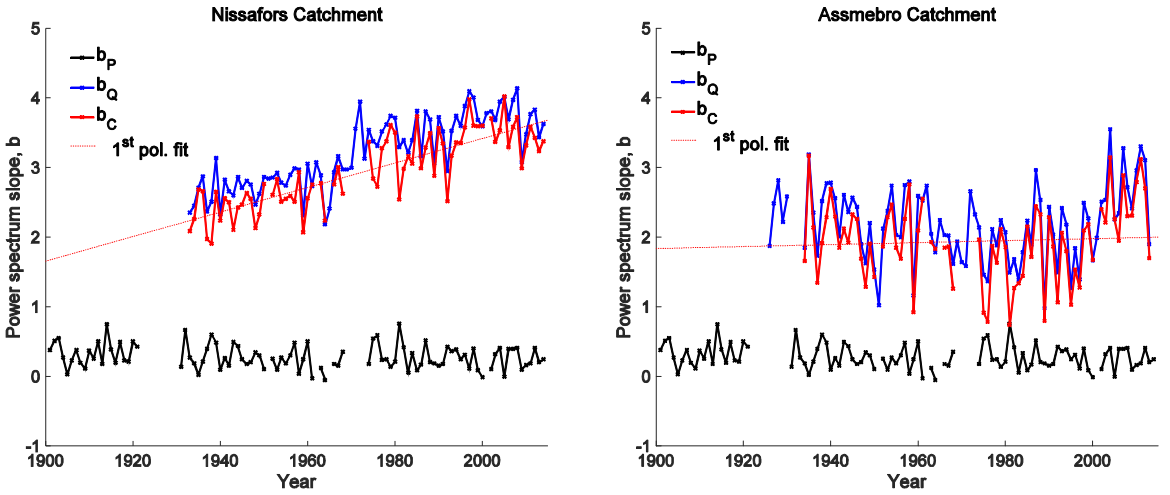

Figure 5. Spectral slope change over the last century in two neighboring catchments (Nissafors and Assmebro) in southwestern Sweden. The temporal changes in the spectral slope for precipitation ($\boldsymbol{b_{P,j}}$, black), discharge ($\boldsymbol{b_{Q,j}}$ blue), and catchment scaling function ($\boldsymbol{b_{C,j}}$, red) are shown for the two catchments. The displayed linear fit is for $\boldsymbol{b_{C,j}}$ and results in the coefficients $k_{b,C}$ and $m_{b,C}$.

in the slope of the discharge power spectrum (Figure 4, left), thereby suggesting that much of the change in the streamflow response is attributable to factors other than temporal changes in precipitation patterns.

Regarding the temporal change in the slope of the catchment scaling function spectrum (i.e., $k_{b,C}$), 26 of the 41 catchments exhibit a statistically significant change at the 95% confidence level. Of these, 24 catchments exhibit an increase (i.e., steepening of the slope of the scaling function over time) and two catchments show a decrease in the slope of the scaling function. Thirty-four of the 41 catchments exhibit a similar trend for the slope of the catchment scaling function as for as the discharge power spectrum (i.e., comparing $k_{b,C}$ with $k_{b,Q}$).

Six catchments exhibit a significant change for discharge power spectrum (S_Q) but not for the catchment scaling function ($S_{f,C}$), whereas one catchment displays the opposite behavior, i.e., a statistically significant change for the scaling function but not for the discharge power spectrum. This discharge station is the Järnforsen station, for which the closest precipitation station is the Västervik station—the only precipitation series that displayed a statistically significant increase ($k_{b,P}$=0.0010, which is smaller than for most catchment scaling functions and the discharge power spectra) in the power spectral slope, i.e., $k_{b,P}$ for the May–October period for the included years.

The temporal change in the slope of the catchment scaling function ($k_{b,C}$) for all 41 catchments for which the precipitation was available, has an average value of 0.0050. The confidence interval, which was calculated via *t*-statistics, varies from 0.0028 to 0.0069, implying that this increase is significant at the 95% confidence level, similarly to the findings for $k_{b,Q}$. Thus, the statistically significant change in the catchment scaling function can predominantly be attributed to other changes than change in the precipitation pattern.

3.2. Stream Network Properties—Different Cartographic Representations

Present-day network representations in the two resolutions and a historical map from the 1880s are shown in Figure 6. These images are accompanied by a present-day land use map in which agricultural land uses are marked in yellow.

Physical properties of the three stream networks are presented in Table 1. When considering the average distance to the catchment outlet, it is clear that the historical map exhibits a larger value than both modern maps, thus supporting the hypothesis that the network flow distance decreased over time.

After comparing the historical stream network coordinates with the two present-day ones, we were confronted with uncertainties regarding the map resolution of the historical map, problems regarding how this map should be compared to modern maps arose; i.e., whether an identified change may have resulted from different map-drawing procedures or from actual physical variations in the catchment. However, the fact that the stream network flow path variance appears to have declined over time also suggests that the

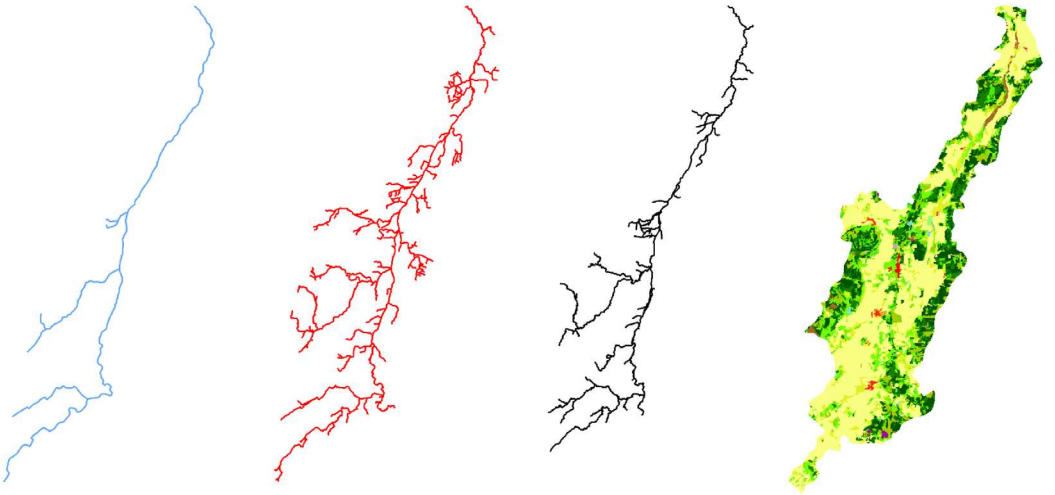

Figure 6. Stream network representation of the Törnestorp Catchment, from left to right: the overview map (present day, blue), the terrain map (present day, red), the historical map (the 1880s, black), and a land use map of present-day conditions.

network has become less branched. Hence, the resolution issue does not appear to constitute a major problem because a temporal change is observed regardless of whether the historical map is compared to a map of lower (the overview map) or higher (the terrain map) resolution. Previous studies have claimed that although these historical maps can be associated with uncertainties related to minor geometrical irregularities and inconsistent classifications, they are typically very accurate for smaller areas on the order of a few square kilometers [*Cousins et al*., 2015].

However, no evidence of the suggested temporal change is revealed when only comparing $CV_X{}^2$-values, thus indicating that this measure is more sensitive to the resolution issue than the average distances. The average slope within the stream network is determined by dividing the average elevation difference between the stream reach's starting point and the catchment outlet with the average flow paths' lengths. These results indicate that the historical map yields the mildest slopes, whereas the overview map has the steepest bottom slope.

3.3. Scenario Analyses—Stream Network Properties and Travel Times

From the distributed stream network routing model and the ensemble of travel times through the stream network for the applied source terms, the average travel flow through the stream network can be derived for each of the various scenarios. A selection of outcomes from the 36 scenarios is presented in Table 2 and Figure 7 to highlight the variations in stream network behaviors resulting from differences in stream network properties. The average travel times compiled in Table 2 can be considered as a presentation of the different scenarios (as they are referred in Figure 7) and also as a description of a snapshot of the travel times because they are valid for the particular outlet discharge of 5 m^3/s. This discharge, while statistically falling within a higher range (the 95th percentile), is not very extreme with respect to its magnitude; the highest recorded discharge in Törnestorp is 27.7 m^3/s. While the generality of this snapshot is difficult to assess, it allows us to distinguish between the scenarios, although at only one particular outlet discharge.

Table 1. Average Geomorphological Properties for the Stream Network Derived From the Three Different Map Representations

	Overview	Terrain	Historical
Number of stream tributaries	11	285	119
Total network distance (m)	63,371	190,950	125,940
Average distance to outlet (m)	23,683	22,821	25,523
Variance, distance to outlet (m^2)	1.29×10^8	1.07×10^8	1.39×10^8
Squared coefficient of variation flow paths $CV_X{}^2$	0.230	0.205	0.214
Average elevation difference (reach to outlet) divided by average distance (for $\Delta x = 100$ m)	0.00206	0.00199	0.00186

Table 2. An Overview of the Average Travel Time Through the Network at the Outlet Discharge of 5.0 m^3/s for the 36 Different Scenarios[a]

	Average Travel Time (h)/Scenario ID							
	Width Increases With Discharge				Width Varies Randomly			
	β = 5° (Floodplain)		β = 90° (Bounded)		β = 5° (Floodplain)		β = 90° (Bounded)	
Overview: $\Delta x = 10$ m	86.1	O_1	21.8	O_4	87.0	O_7	26.3	O_{10}
Terrain: $\Delta x = 10$ m	176	T_1	28.0	T_4	180	T_7	33.9	T_{10}
Historical: $\Delta x = 10$ m	180	H_1	31.1	H_4	185	H_7	37.6	H_{10}
Overview: $\Delta x = 50$ m	76.7	O_2	22.1	O_5	77.2	O_8	27.2	O_{11}
Terrain: $\Delta x = 50$ m	150	T_1	27.7	T_5	154	T_8	34.8	T_{11}
Historical: $\Delta x = 50$ m	156	H_2	30.0	H_5	144	H_8	34.1	H_{11}
Overview: $\Delta x = 100$ m	71.8	O_3	22.0	O_6	71.4	O_9	24.4	O_{12}
Terrain: $\Delta x = 100$ m	132	T_1	26.4	T_6	134	T_9	31.3	T_{12}
Historical: $\Delta x = 100$ m	200	H_3	31.5	H_6	203	H_9	36.1	H_{12}

[a]As a comparison, the average discharge in the Törnestorp Catchment is 1.58 m^3/s, and a value of 5.0 m^3/s over the 60 year observational series corresponds to the 95th percentile. Each scenario is coded by an index number and letter denoting the map from which network coordinates were obtained. O indicates the overview map, T indicates the terrain map, and H indicates the historical map. The index letter and number of each scenario is included in italics.

From Table 2 and Figure 7, it is evident that the stream network properties have a considerable impact on the average travel time through the catchment. However, because the table only presents the travel times for one particular flow, it is difficult to fully appreciate the complex interactions among stream network properties because the relative difference between the different scenarios varies with the discharge.

The top left subplot in Figure 7 shows that the average travel time generally decreases with decreasing Δx. The general slope of the landscape is positive, and as the resolution decreases, a relatively smaller share of the total flow length will have a low or negative slope (resulting in slow flow velocities) which reduces the in-stream travel time. The top right subplot of Figure 7 shows that the travel times become longer when floodplain geometries are used instead of bounded geometries and that this property has a profound influence on the average travel times. The bottom left subplot shows the effects of stream channel widths,

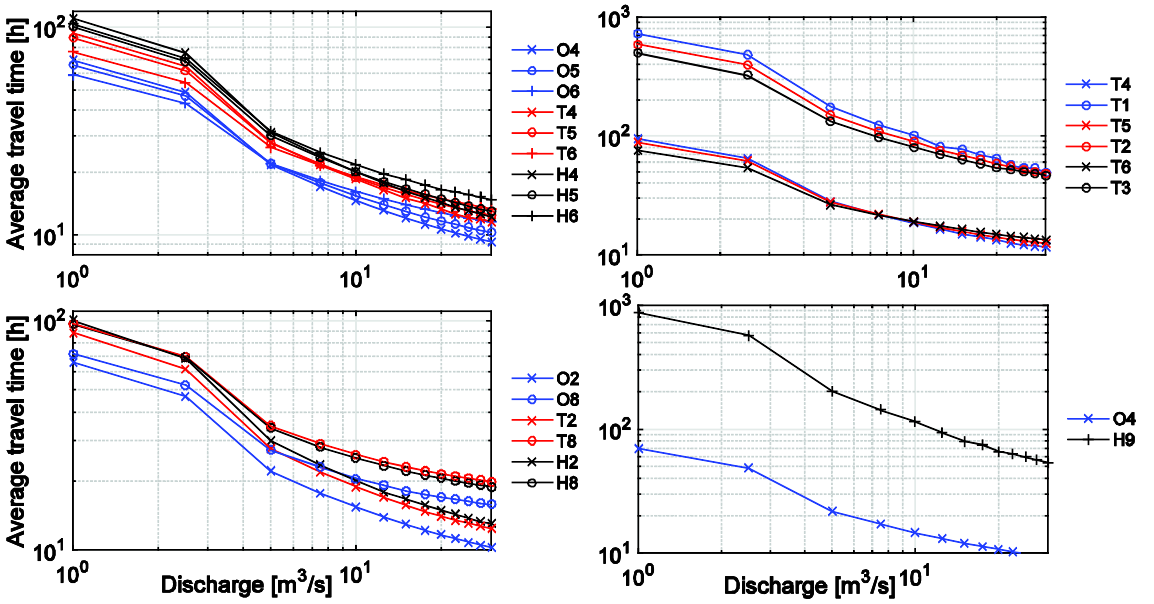

Figure 7. Average travel times ($\langle\tau(\boldsymbol{Q_{in}})\rangle$) according to the implications of various factors, presented as scenarios according to Table 2: (a) (top left) implications of different stream network representations and reach length resolutions, (b) (top right) implications of cross-sectional geometries, (c) implications of stream widths that do not increase uniformly with the discharge, and (d) differences between the slowest (scenario H9) and fastest (scenario O4).

revealing that travel times are consistently longer when randomized values of stream channel width (w_{rand}) are used than when the widths (w) increase uniformly with discharge. This is a result of the narrow bottlenecks obstructing the water flow and reducing the flow velocities when widths are varying. The bottom right subplot of Figure 7 presents the difference between the fastest (scenario O4) and slowest (scenario H9) scenarios among the 36 studied scenarios—which highlights the interconnection between stream network properties and in-stream travel times.

3.4. Discharge Modeling Using Different Stream Network Flow Response Functions

The effects of stream network properties on streamflow responses can be quantified using the $\langle \tau(Q) \rangle$ relationships to parameterize the hydrological model (cf. equation (16)) which allows for comparisons of the outflow hydrographs resulting from the different routing scenarios. The general agreement between the observed and simulated discharges was evaluated using the Nash-Sutcliffe model efficiency index (R_{eff}), which revealed that the outcomes of the physically based routing model were similar to those of the HBV-modeling, resulting in R_{eff} values of 0.50–0.55.

Another method of comparing the performance of the model approaches that are based on the traditional stream network flow response function and the nonlinear representation derived from the flow routing (section 2.3.2) involves comparing the power spectra of the stream network scaling function $S_{f,N}$ (see equation (13)). A comparison of the discharge predictions resulting from (i) the HBV model with its usual routing routine and (ii) the HBV model with the physically based routing routine (scenario O6) is displayed in Figure 8. For both parameterization types, the best-performing (according to R_{eff}) parameterizations were used.

In both models, the relative influence of stream network processes is observed to increase with decreasing time scale, and this difference diminishes for the longer time scales, i.e., when the stream network scaling function $S_{f,N}$ approaches unity. When using the physically based stream network flow response function, the power spectrum of the modeled outflow becomes more similar to the observed (measured) discharge hydrograph because the HBV routing routine in this application dampens the hydrograph too extensively. This difference is most apparent for short periods, for which the stream network scaling function is roughly 1 order of magnitude higher when using the physically based parameterization than in the HBV formulation.

4. Discussion

4.1. Spectral Analyses of the Catchment Flow Response

The spectral analysis has the advantage of displaying trends that would be difficult to distinguish and quantify if only investigating the hydrographs themselves (in the time domain). Patterns that are not otherwise clearly observable can emerge when then the information is decomposed on different frequencies or periods. Therefore, a major shift in the power spectrum for a certain period may not be apparent in the discharge data because the hydrographs display the superimposed effect of all possible time scales.

A large number of factors can influence the streamflow response of a catchment, and many of these factors interact in a complex manner. The results, which are presented as changes in the discharge power spectral slope, are thus difficult to directly correlate with specific land use changes.

For the areas in which intense agriculture is occurring, development over the last century has involved developments toward intensified, large-scale agriculture including enhanced drainage of wetlands, lowering of lake levels, levee construction, stream excavation, straightening, etc. [*Cousins et al*., 2015; *Blöschl et al*., 2015; *Hall et al*., 2014; *Ihse*, 1995; *Jaramillo et al*., 2013; *Jepsen et al*., 2015; *Jordbruksverket*, 2011]. In the Västergötland region where Törnestorp Catchment is located, the average cultivated area per farm has increased approximately four times since the 1930s and the area of pipe-drained areal land has increased five times [*Jordbruksverket*, 2011]. Other possible anthropogenically induced causes of the changes in power spectra, could be gradual changes in crop practice, however, usually such technology related changes are more rapid than the gradual change in the power spectrum of the hydrograph. Scrutinizing Figure 5 for Nissafors (left subplot), a shift might be present around 1970 which coincides with changes made to the measuring station. Although this may indicate a sudden change of conditions, the gradual increase of the spectrum slope is nonetheless persistent before as well as after 1970.

In the northernmost catchments, a possible explanation for the temporal changes in the discharge power spectrum may relate to the thawing of permafrost because of climate change-induced temperature increases, as several of the catchments exhibiting significant increases in discharge power spectral slopes have exhibited indications of permafrost thawing [*Sjöberg et al*., 2012]. Even in May and June (months that were included in the spectral analyses), spring floods caused by snowmelt may significantly affect the hydrographs in the northernmost catchments. This brings into question the validity of Equation (5) for these instances. Spectral slope changes can also depend on the presence of lakes. The large water volumes present in lakes will generally result in high attenuation for a water pulse through a given catchment, i.e., the presence of a lake can overshadow any eventual land use changes in subcatchments draining into the lake [*Schulze et al*., 2005]. In many catchments, some degree of regulation may also be present, even if not actively applied. In general, changes due to regulation are manifested as a decrease in the long-term variance and an increase in the short-term variance, i.e., a decrease in the slope of the power spectrum [*Wörman et al*. 2010]. Another study of Swedish catchments [*Destouni et al*. 2013] confirms that hydropower has caused decreases in the temporal runoff variability, whereas the non-irrigated agriculture has increased the temporal runoff variability.

Because the two maps in Figure 4 resemble one another, and the power spectrum of precipitation data for the seven examined long-term precipitation records is almost completely flat, the hypothesis that temporal variations in discharge spectra can be largely caused by land use changes within catchments is supported [*Jaramillo et al*., 2013]. This has previously been demonstrated for other geographical regions (e.g., North America) [*Zhang and Schilling*, 2006; *Mao and Cherkauer*, 2009]. The results also suggest that changes in catchment properties can in some cases cause relatively more substantial changes in the streamflow responses than changes in precipitation [*DeFries and Eshleman*, 2004; *Jaramillo and Destouni*, 2014].

Potential limitations of the temporal investigation based on historical discharge series may include sensitivity to years that are meteorologically considered to be nonrepresentative of the time period, which may have considerably affected the results [*Blöschl et al*., 2015]. For example, in Sweden, the 1920s are known to have been cold and wet [*Lindström and Bergström*, 2004; *Wilson et al*., 2010]. Additionally, discharge, temperature and precipitation measurements cannot always be expected to be of comparable quality to more modern measurement techniques [*Lindström and Bergström*, 2004]. Another difficulty is related to the fact that the discharge series for the 79 catchments do not all cover the same time frame. Additionally, the data used to select the suitable unregulated (or at least regulated to a low extent) catchments were relevant to present-day conditions, implying that catchments may have been regulated to a greater extent earlier in the discharge measurement period.

4.2. Scenario Analyses to Quantify Effects of Changes in Stream Network Properties

The outcomes of the distributed routing model for the different scenarios reveal the complex nexus of the geomorphological (distribution of the flow paths' topology and topography), hydrodynamic (cross-sectional geometries) and kinematic (distribution of narrow cross sections, backwater subreaches, etc.) properties [*Saco and Kumar*, 2002]. The scenario with the shortest travel times (scenario O4) is characterized by bounded cross-sectional geometry, dense spatial resolution (low Δx), uniformly increasing river width with discharge and a map representation derived from the overview map, whereas the scenario with the longest travel times (scenario H9) is characterized by floodplain cross-sectional geometry, coarse spatial resolution (large Δx), randomized river width (see Figure 2) and the map representation derived from the historical map. From the stream network routing and synthesis of the stream network travel times according to different stream network properties (scenario), the following general results are found:

1. $<\tau>$ generally decreases with decreasing Δx.
2. $<\tau>$ is longer for the floodplain scenarios than for the bounded scenarios.
3. $<\tau>$ is generally higher for the scenarios with nonuniform cross-sectional widths.
4. The smallest $<\tau>$ (fastest travel times) are always found using representations from the overview map. Typically, the longest travel times are obtained using historical maps. Here it is evident that the travel times depend on the average in-stream distance to the outlet (cf. Tables 1 and 2), which explains why the travel time of the historical network representation is the longest.

4.3. Discharge Modeling Using Different Stream Network Flow Response Functions

Power spectral methods can also be used to evaluate the difference between the stream network flow response functions as modeled by the simpler HBV model routing routine and the physically based routing

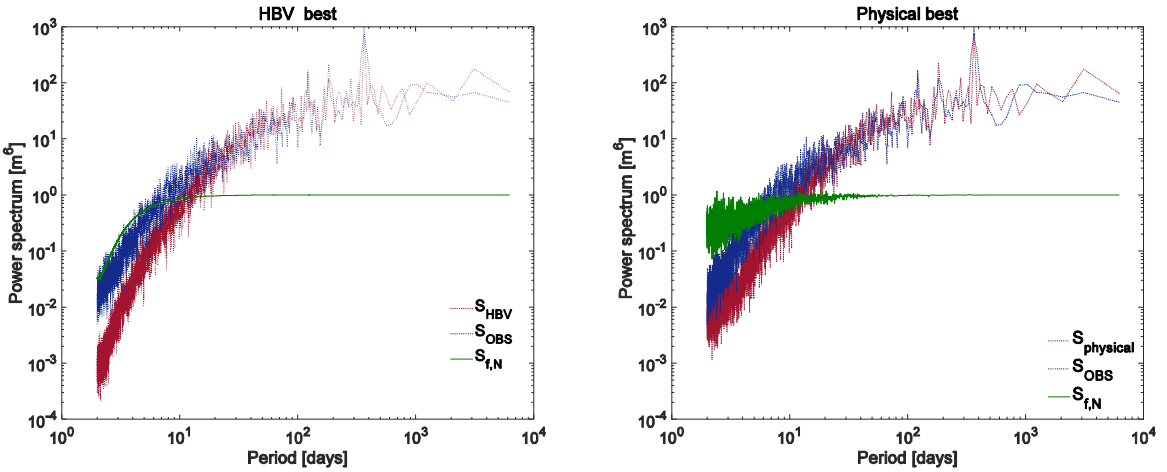

Figure 8. Examples of the spectrum appearance of the observed/measured hydrograph S_{OBS} (blue), the modeled outflowing hydrograph S_{HBV} *or* $S_{physical}$ (dark red), and the stream network scaling function $S_{f,N}$ (green) for the best-performing parameterizations of (left) the HBV model with its usual routing routine and (right) the HBV model with the physically based routing routine, respectively.

model. The findings displayed in Figure 8 show that the routing description provided by the physically based model more resembles the actual routing processes that occur in the stream network than do the routing descriptions in the hydrologic model (HBV). The major difference between the modeled discharges conceived from the two respective models can be observed for the short time scales. Generally, the routing component of the HBV-model (see section 2.3.1) represents a more generic and simplified description of stream network routing mechanisms compared with the physically based stream network flow response function (see section 2.3.2). For the two most extreme modeled scenarios for the Törnestorp case study (O4 and H9; see Figure 7 and Table 2), the stream network scaling function was similar between both modeled scenarios, implying that they both appear to adequately represent the streamflow routing mechanisms.

The use of stage-dependent stream network flow response functions yields a larger spread of discharges, with a higher occurrence of extreme values, thus potentially being better suited to model peak flows. The power spectra presented in Figure 8, thus, illuminates a fundamental difference between different streamflow routing models decomposed on periods. This approach facilitates a discrimination of model performances in a manner that is not achieved by comparing the R_{eff} values, which were similar for most modeled scenarios.

The power spectrum of the modeled discharge using the physically based stream network flow response function showed greater consistency with the measured hydrographs and indicates that the routing description of the HVB model generally underestimates the flow peaks, resulting in an exaggerated damping of the streamflow response.

4.4. Change in Streamflow Response—Analytical Interpretation of the Stream Network Scaling Function

A key factor in determining the shape of the IUH (and consequently the stream network scaling function) is the relative importance of different dispersion mechanisms associated with both the geomorphology and hydrodynamics of the network [*Rinaldo et al*., 1991; *Saco and Kumar*, 2002; *Riml and Wörman*, 2011; *Rodriguez-Iturbe/Rinaldo*, 1996, 2001]. Shifts over time in the relative importance of these mechanisms will affect the shape of the stream network flow response (and consequently the stream network scaling function).

By using the stream network data from the historical map representation of Törnestorp with $\alpha_\gamma = 4.67$ and $\beta_\gamma = 1.84 \times 10^{-4}$ m^{-1} together with an assumed stream flow velocity $u = 0.5$ m/s, the theoretical implications of a changed hydrodynamical dispersion for the Törnestorp stream network were investigated (Figure 9) using equation (14) and a numerical inverse Laplace transform [*Hollenbeck*, 1998] of equation (15).

As exemplified by Figure 9, complex variation in the relative importance of the geomorphological and hydrodynamic dispersion results in a nonmonotonic change in the peak value of the stream network flow response $f_{N,\max}$. The green lines represent a case where the flow response is dominated by geomorphological dispersion and the blue lines represent a flow response dominated by hydrodynamical dispersion.

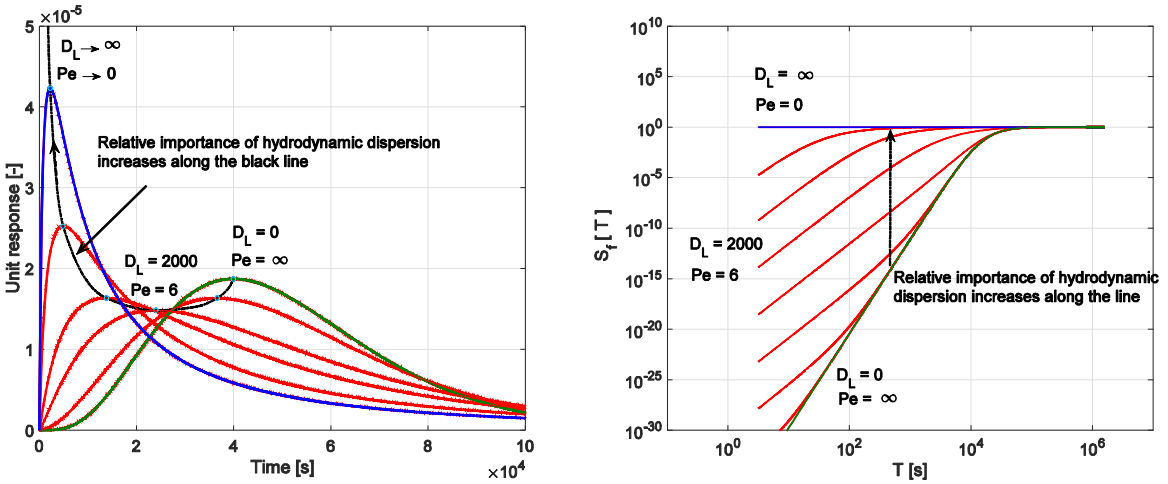

Figure 9. (left) Unit stream network response and (right) the stream network scaling function and their dependency on the hydrodynamic dispersion, D_L, for the Törnestorp stream network. The green lines represent a case where geomorphological dispersion is dominating over hydrodynamical dispersion (blue lines). The maximum values of (left subplot) each unit response curve are interconnected and the dashed black line shows how (left) $f_{N,max}$ and (right) the scaling function changes with increasing importance of the hydrodynamic dispersion.

Theoretically, this means that a change in D_L (or in the Péclet number, $Pe = \alpha \cdot u/(\beta \cdot D_L)$) could result in either an increase or decrease in $f_{N,\max}$ and that additional independent observations of the catchment network structure and *Pe*-number regime are needed to draw any conclusions regarding how the *Pe*-number affects the stream network flow response. However, when the geomorphological dispersion dominates over hydrodynamic dispersion, which is often the case regardless of the spatial scale due to the self-similar topologies of stream networks [*Saco and Kumar*, 2002], a decrease in D_L (or increase in *Pe*) will lead to an increase in $f_{N,\max}$. This interpretation is supported by the scenario analyses of the case study, Törnestorp Catchment, which revealed D_L values < 800 m^2/s even for very large discharge values, indicating a regime where geomorphological dispersion always dominates (Figure 9). Thus, the lowering of the catchment scaling function $S_{f,C}$ at short periods observed in many Swedish catchments over the last century (i.e., steepening of the slope of the catchment scaling function) is likely caused by a decrease in D_L (increase in *Pe*) over time, resulting in higher peak values, especially for rapid streamflow responses (i.e., over short periods).

4.5. Change in Streamflow Response—Numerical Interpretation in the Case Study

The hydrodynamical dispersion coefficient can be approximated as a function of the average water level *y* (m) and the slope of the energy line S_0 as $D_L = u \cdot y/(3 \cdot S_0)$ [*Rinaldo et al.*, 1991]. The outcome of the map analyses of the Törnestorp Catchment indicates that S_0 has increased over time. The outcomes from the distributed routing (based on the scenario modeling) indicate that *y* has decreased over time, as it is generally lower for all present-day scenarios. Together, this implies that the *Pe*-number has increased over time which is the explanation for the steepening of the catchment scaling function (cf. Figure 9, left subplot), and consequently also the discharge power spectrum, over time.

The scenario modeling suggests that many anthropogenic modifications in agricultural landscapes can significantly affect the hydrograph variations. Such drainage measures include lowering of average stage, flow path lengths, hydrodynamical dispersion, and/or increases in flow velocities or bed slopes. These measures in streams generally cause increasing *Pe*-numbers and a lowering of the short-term temporal variance in hydrographs. All of the analytically and numerically derived findings correspond well with the basic conception that farmers in these types of agricultural areas have generally wanted to avoid flooding, hence facilitating drainage by reducing water levels and increasing flow velocities.

5. Conclusions

A Fourier spectral analysis of 55–110 years of daily discharge time series from 79 unregulated catchments in Sweden revealed that the discharge power spectrum slope has in general increased gradually over time. The increase was significant in 58 of the 79 catchments as well as nationally for the ensemble of all

catchments. Decreases in the discharge power spectrum were generally observed for short periods (high frequencies). The results also indicated that the catchment scaling function (i.e., the power spectrum of the IUH) had steepened in most of the 41 southernmost catchments for which historical precipitation time series were available.

Interpretation of an exact solution to the discharge power spectra (equation (6)) indicate that local land use changes within the catchments have affected discharge power spectra to a greater extent than have changes in precipitation patterns. The change is probably caused by changes in hydrodynamical and/or geomorphological dispersion factors that are due to anthropogenic and/or natural causes.

Routing analyses that were based on historical and current maps demonstrated the relationship between catchment characteristics and stream network scaling function. The analyses showed that a change in stream network properties, reflected in the Péclet number (and hence D_L), can result in changes in the power spectra, where the relative importance of the geomorphological and hydrodynamic dispersion effects determine the shape of the streamflow response. The lowering of the catchment scaling function $S_{f,C}$ observed in many Swedish catchments over the last century is likely caused by a decrease in D_L (increase in *Pe*) over time resulting in higher peak values especially for rapid streamflow responses (i.e., over short periods), demonstrated empirically for the Törnestorp case study.

The analysis of historical maps from the Törnestorp Catchment and scenario modeling suggests that (anthropogenic) changes in the properties of a stream network can cause substantial changes in the discharge power spectra. For the Törnestorp Catchment, the average flow length and water level (as demonstrated through 1-D distributed routing analysis) were shown to decrease over time, whereas the average bottom slope was shown to increase.

The Péclet number was thus shown to have increased over time, resulting in a lowering of the discharge power spectrum for the short periods. Observed and modeled changes are qualitatively consistent with the exact, spectral solution to the stream network scaling function which shows that when geomorphological dispersion is dominating over hydrodynamic dispersion a decrease in D_L (or increase in *Pe*) will lead to a lowering of the power spectra for short periods, and resulting in peakier hydrographs.

The analyses also showed that the stream network scaling function is higher for shorter time periods when a nonlinear physically based stream network flow response function is used compared with when stream network flow response of the HBV model. This result was observed despite the fact that the two routing methodologies show similar levels of performance in terms of their R_{eff}-values of the entire discharge series, which implies that deviations in model performance over short periods (short-term fluctuations) are not well reflected when solely using the R_{eff} measures.

The power spectra can change significantly over time due to changes in stream network properties that change the Péclet numbers. This emphasizes the need for hydrological models to account for the effect of the nonstationarity of parameters that result from temporal change caused by land use change and/or climate change that is due to anthropogenic or natural causes.

Acknowledgments

This study was financially supported by Elforsk AB, as a part of the research activities of the Swedish Hydropower Centre (SVC). Thanks are also due to Göran Lindström and his colleagues at the Swedish Meteorological and Hydrological Institute (SMHI) for their cooperation. The historical discharge data for the 79 catchments are publicly available at http://vattenweb.smhi.se/station/. The code used to make the figures and to achieve all presented results, as well as the reported results themselves, will be preserved in a long-term storage system. These items will be made available upon request to the corresponding author, Anna Åkesson (anake@kth.se). The authors thank the three anonymous reviewers for their insightful comments that helped improve this article.

References

Åkesson, A., and A. Wörman (2012), Stage-dependent hydraulic and hydromorphologic properties in stream networks translated into response functions of compartmental models, *J. Hydrol.*, *420–421*, 25–36, doi:10.1016/j.jhydrol.2011.11.015.

Åkesson, A., A. Wörman, and A. Bottacin-Busolin (2015), Hydraulic response in flooded stream networks, *Water Resour. Res.*, *51*, 213–240, doi:10.1002/2014WR016279.

Arcement, G. J., and V. R. Schneider (1989), Guide for selecting Manning's roughness coefficients for natural channels and flood plains. *U.S. Geol. Surv. Water Supply Pap.*, 2339, 38 pp.

Basu, N. B., S. E. Thompson, and P. S. Rao (2011), Hydrologic and biogeochemical functioning of intensively managed catchments: A synthesis of top-down analyses, *Water Resour. Res.*, *48*, W00J15, doi:10.1029/2011WR010800.

Benettin, P., J. W. Kirchner, A. Rinaldo, and G. Botter (2015), Modeling chloride transport using travel time distributions at Plynlimon, Wales, *Water Resour. Res.*, *51*, 3259–3276, doi:10.1002/2014WR016600.

Bergström, S., and A. Forsman (1973), Development of a conceptual deterministic rainfall-runoff model, *Nord. Hydrol.*, *4*, 147–170.

Bergström, S., B. Carlsson, M. Gardelin, G. Lindstrom, A. Pettersson, and M. Rummukainen (2001), Climate change impacts on runoff in Sweden—Assessments by global climate models, dynamical downscaling and hydrological modeling, *Clim. Res.*, *16*, 101–112.

Blöschl, G., et al. (2015), Increasing river floods: Fiction or reality?, *WIREs Water*, *2*, 329–344, doi:10.1002/wat2.1079.

Chow, V. T., D. Maidment, and L. Mays (1988), *Applied Hydrology*, McGraw-Hill Ser. Water Resour. Environ. Eng.

Cousins, S. A. O., A. G. Auffret, J. Lindgren, and L. Tränk (2015), Regional-scale land-cover change during the 20th century and its consequences for biodiversity, *Ambio*, *44*, 17–27, doi:10.1007/s13280-014-0585-9.

DeFries, R., and K. N. Eshleman (2004), Land-use change and hydrologic processes: A major focus for the future, *Hydrol. Processes*, *18*, 2183–2186, doi:10.1002/hyp.5584.
Destouni, G., F. Jaramillo, and C. Prieto (2013), Hydroclimatic shifts driven by human water use for food and energy production, *Nat. Clim. Change*, *3*, 213–217, doi:10.1038/nclimate1719.
Dolgonosov, B. M., K. A. Korchagin, and N. V. Kirpichnikova (2008), Modeling of annual oscillations and 1/f-noise of daily river discharges, *J. Hydrol.*, *357*, 174–187, doi:10.1016/j.jhydrol.2008.04.023.
Dooge, J. C. I. (1959), A general theory of the unit hydrograph, *J. Geophys. Res.*, *64*, 241–256, doi:10.1029/JZ064i002p00241.
Foster, M., R. Fell, and M. Spannagle (2000), The statistics of embankment dam failures and accidents, *Can. Geotech. J.*, *37*, 1000–1024, doi:10.1139/t00-030.
French, R. (2007), *Open Channel Hydraulics*, 1st ed., McGraw-Hill, N. Y.
Giorgi, F., C. Shields Brodeur, and G. T. Bates (1994), Regional climate change scenarios over the United States produced with a nested regional climate model, *J. Clim.*, *7*, 375–399, doi:10.1175/1520-0442(1994)007 < 0375:RCCSOT>2.0.CO;2.
Hall, J., et al. (2014), Understanding flood regime changes in Europe: A state-of-the-art assessment, *Hydrol. Earth Syst. Sci.*, *18*, 2735–2772, doi:10.5194/hess-18-2735-2014.
Harman, C. J. (2015), Time-variable transit time distributions and transport: Theory and application to storage-dependent transport of chloride in a watershed, *Water Resour. Res.*, *51*, 1–30, doi:10.1002/2014WR015707.
Hirsch, R. M., and S. A. Archfield (2015), Flood trends: Not higher but more often, *Nat. Clim. Change*, *5*, 198–199, doi:10.1038/nclimate2551.
Hollenbeck, K. J. (1998), INVLAP.m: A MATLAB function for numerical inversion of Laplace transforms by the de Hoog algorithm. [Available at http://www.isva.dtu.dk/staff/karl/invlap.html.]
Ihse, M. (1995), Swedish agricultural landscapes—Patterns and changes during the last 50 years, studied by aerial photos, *Landscape Urban Plan.*, *31*, 21–37, doi:10.1016/0169-2046(94)01033-5.
Jaramillo, F., and G. Destouni (2014), Developing water change spectra and distinguishing change drivers worldwide, *Geophys. Res. Lett.*, *41*, 8377–8386, doi:10.1002/2014GL061848.
Jaramillo, F., C. Prieto, S. W. Lyon, and G. Destouni (2013), Multimethod assessment of evapotranspiration shifts due to non-irrigated agricultural development in Sweden, *J. Hydrol.*, *484*, 55–62, doi:10.1016/j.jhydrol.2013.01.010.
Jepsen, M. R., et al. (2015), Transitions in European land management regimes between 1800 and 2010, *Land Use Policy*, *49*, 53–64, doi:10.1016/j.landusepol.2015.07.003.
Jordbruksverket (2011), *Jordbruket i siffror: åren 1866–2007, Tabellbilaga, Jordbruksverket*, Jönköping, Sweden.
Kirchner, J. W. (2009), Catchments as simple dynamical systems: Catchment characterization, rainfall-runoff modeling, and doing hydrology backward, *Water Resour. Res.*, *45*, W02429, doi:10.1029/2008WR006912.
Kirchner, J. W., X. Feng, and C. Neal (2000), Fractal stream chemistry and its implications for contaminant transport in catchments, *Nature*, *403*, 524–527, doi:10.1038/35000537.
Kløve, B., and L. Bengtsson (1999), Runoff generation in a plough-drained cutover fen in Central Finland, *J. Hydrol.*, *218*, 157–168, doi:10.1016/S0022-1694(99)00036-0.
Lindström, G., and S. Bergström (2004), Runoff trends in Sweden 1807–2002, *Hydrol. Sci. J.*, *49*, 69–83.
Lindström, G., B. Johansson, M. Persson, M. Gardelin, and S. Bergström (1997), Development and test of the distributed HBV-96 hydrological model, *J. Hydrol.*, *201*, 272–288, doi:10.1016/S0022-1694(97)00041-3.
Lindström, G., C. Pers, J. Rosberg, J. Strömqvist, and B. Arheimer (2010), Development and testing of the HYPE (Hydrological Predictions for the Environment) water quality model for different spatial scales, *Hydrol. Res.*, *41*, 295–319, doi:10.2166/nh.2010.007.
Liu, Y. B., S. Gebremeskel, F. De Smedt, L. Hoffmann, and L. Pfister (2003), A diffusive transport approach for flow routing in GIS-based flood modeling, *J. Hydrol.*, *283*, 91–106, doi:10.1016/S0022-1694(03)00242-7.
Mao, D., and K. A. Cherkauer (2009), Impacts of land-use change on hydrologic responses in the Great Lakes region, *J. Hydrol.*, *374*, 71–82, doi:10.1016/j.jhydrol.2009.06.016.
McDonnell, J. J., et al. (2010), How old is streamwater? Open questions in catchment transit time conceptualization, modeling and analysis, *Hydrol. Processes*, *24*, 1745–1754, doi:10.1002/hyp.7796.
Montanari, A., et al. (2013), "Panta Rhei—Everything Flows": Change in hydrology and society—The IAHS Scientific Decade 2013–2022, *Hydrol. Sci. J.*, *58*, 1256–1275.
Nash, J. E., and J. V. Sutcliffe (1970), River flow forecasting through conceptual models part I—A discussion of principles, *J. Hydrol.*, *10*, 282–290, doi:10.1016/0022-1694(70)90255-6.
Niehoff, D., U. Fritsch, and A. Bronstert (2002), Land-use impacts on storm-runoff generation: Scenarios of land-use change and simulation of hydrological response in a meso-scale catchment in SW-Germany, *J. Hydrol.*, *267*, 80–93, doi:10.1016/S0022-1694(02)00142-7.
Palanisamy, B., and S. R. Workman (2014), Observed hydrographs: On their ability to infer a time-invariant hydrological transfer function for flow prediction in ungauged basins, *Hydrol. Processes*, *28*, 401–413, doi:10.1002/hyp.9583.
Riml, J., and A. Wörman (2011), Response functions for in-stream solute transport in river networks, *Water Resour. Res.*, *47*, W06502, doi:10.1029/2010WR009412.
Riml, J., and A. Wörman (2015), Spatiotemporal decomposition of solute dispersion in watersheds, *Water Resour. Res.*, *51*, 2377–2392, doi:10.1002/2014WR016385.
Rinaldo, A., A. Marani, and R. Rigon (1991), Geomorphological dispersion, *Water Resour. Res.*, *27*, 513–525.
Rodríguez-Iturbe, I., and A. Rinaldo (1996), Geomorphological theory of the hydrological response, *Hydrol. Processes*, *10*, 803–829, doi:10.1002/(SICI)1099-1085(199606)10:6<803::AID-HYP373>3.0.CO;2-N.
Rodríguez-Iturbe, I., and A. Rinaldo (2001), *Fractal River Basins: Chance and Self-Organization*, New ed., Cambridge Univ. Press, Cambridge, U. K.
Rodríguez-Iturbe, I., and J. B. Valdés (1979), The geomorphologic structure of hydrologic response, *Water Resour. Res.*, *15*, 1409–1420, doi:10.1029/WR015i006p01409.
Saco, P. M., and P. Kumar (2002), Kinematic dispersion in stream networks: 2. Scale issues and self-similar network organization, *Water Resour. Res.*, *38*(11), 1245, doi:10.1029/2001WR000694.
Salehin, M., A. I. Packman, and A. Wörman (2003), Comparison of transient storage in vegetated and unvegetated reaches of a small agricultural stream in Sweden: Seasonal variation and anthropogenic manipulation, *Adv. Water Resour.*, *26*, 951–964, doi:10.1016/S0309-1708(03)00084-8.
Schulze, K., M. Hunger, and P. Döll (2005), Simulating river flow velocity on global scale, *Adv. Geosci.*, *5*, 133–136, doi:10.5194/adgeo-5-133-2005.
Seibert, J. (1997), Estimation of parameter uncertainty in the HBV model, *Nord. Hydrol.*, *28*(4/5), 247–262.

Seibert, J. (2000), Multi-criteria calibration of a conceptual runoff model using a genetic algorithm, *Hydrol. Earth Syst. Sci.*, *4*, 215–224, doi: 10.5194/hess-4-215-2000.
Seibert, J., and M. J. P. Vis (2012), Teaching hydrological modeling with a user-friendly catchment-runoff-model software package, *Hydrol. Earth Syst. Sci.*, *16*, 3315–3325, doi:10.5194/hess-16-3315-2012.
Sjöberg, Y., A. Frampton, and S. W. Lyon (2012), Using streamflow characteristics to explore permafrost thawing in northern Swedish catchments, *Hydrogeol. J.*, *21*, 121–131, doi:10.1007/s10040-012-0932-5.
Snell, J., and M. Sivapalan (1994), On geomorphological dispersion in natural catchments and the geomorphological unit hydrograph, *Water Resour. Res.*, *30*, 2311–2323, doi:10.1029/94WR00537.
Steinschneider, S., and C. Brown (2013), A semiparametric multivariate, multisite weather generator with low-frequency variability for use in climate risk assessments, *Water Resour. Res.*, *49*, 7205–7220, doi:10.1002/wrcr.20528.
Teutschbein, C., and J. Seibert (2013), Is bias correction of regional climate model (RCM) simulations possible for non-stationary conditions?, *Hydrol. Earth Syst. Sci.*, *17*, 5061–5077, doi:10.5194/hess-17-5061-2013.
Torrence, C., and G. P. Compo (1998), A practical guide to wavelet analysis, *Bull. Am. Meteorol. Soc.*, *79*, 61–78.
Troutman, B. M., and M. R. Karlinger (1984), On the expected width function for topologically random channel networks, *J. Appl. Probab.*, *21*, 836–849, doi:10.2307/3213700.
Viglione, A., G. B. Chirico, R. Woods, and G. Blöschl (2010), Generalised synthesis of space–time variability in flood response: An analytical framework, *J. Hydrol.*, *394*, 198–212, doi:10.1016/j.jhydrol.2010.05.047.
Vörösmarty, C., P. Green, J. Salisbury, and R. Lammers (2000), Global water resources: Vulnerability from climate change and population growth, *Science*, *289*, 284–288.
Wagener, T., M. Sivapalan, P. A. Troch, B. L. McGlynn, C. J. Harman, H. V. Gupta, P. Kumar, P. S. C. Rao, N. B. Basu, and J. S. Wilson (2010), The future of hydrology: An evolving science for a changing world, *Water Resour. Res.*, *46*, W05301, doi:10.1029/2009WR008906.
Wang, G., T. Jiang, R. Blender, and K. Fraedrich (2008), Yangtze 1/f discharge variability and the interacting river–lake system, *J. Hydrol.*, *351*, 230–237, doi:10.1016/j.jhydrol.2007.12.016.
Wilson, D., H. Hisdal, and D. Lawrence (2010), Has streamflow changed in the Nordic countries?—Recent trends and comparisons to hydrological projections, *J. Hydrol.*, *394*, 334–346, doi:10.1016/j.jhydrol.2010.09.010.
Wörman, A., G. Lindström, A. Åkesson, and J. Riml (2010), Drifting runoff periodicity during the 20th century due to changing surface water volume, *Hydrol. Processes*, *24*, 3772–3784, doi:10.1002/hyp.7810.
Xu, C. (1999), From GCMs to river flow: A review of downscaling methods and hydrologic modeling approaches, *Prog. Phys. Geogr.*, *23*, 229–249, doi:10.1177/030913339902300204.
Zhang, Y.-K., and K. E. Schilling (2006), Increasing streamflow and baseflow in Mississippi River since the 1940 s: Effect of land use change, *J. Hydrol.*, *324*, 412–422, doi:10.1016/j.jhydrol.2005.09.033.